Simulation of a supercellular storm using a three-dimensional mesoscae model with an explicit lightning flash scheme

Christelle Barthe, Jean-Pierre Pinty

Simulation of a supercellular storm using a three-dimensional mesoscale model with an explicit lightning flash scheme

Christelle Barthe[1] and Jean-Pierre Pinty[1]

Received 5 May 2006; revised 28 September 2006; accepted 2 November 2006; published 28 March 2007.

[1] A complete lightning flash scheme is implemented in the three-dimensional (3-D) nonhydrostatic mesoscale model Méso-NH of the French community. The scheme, which is part of the electrical scheme, follows a new approach with two steps. First, lightning flashes are modeled as bidirectional leaders to mimic the vertical propagation of the initial discharge channels along the electric field. Then, a probabilistic branching algorithm is adapted from the dielectric breakdown concept to reinforce the flash propagation toward distant regions of high charge density but immersed in a weak electric field. This results in a high increase of the total length of the lightning flash channel and also in a better capture of the morphology of intracloud lightning flashes. The electrification and lightning schemes are tested for an ideal case of a supercellular storm. The model succeeds in reproducing the general features of a storm and the electric charge cycle. Sensitivity analyses show that the implementation of a branching stage is necessary and efficient enough to relax the growth of the electric field. The intracloud discharges generated by the model look realistic with a two-layer horizontal structure extending over tens of kilometers from the triggering area. The lightning flash length and the quantity of charge neutralized are ten times more important when the branching algorithm is taken into account. The main conclusion drawn from this study is the feasibility and the benefit of an advanced treatment of lightning flashes in 3-D numerical simulations with an electrification scheme.

Citation: Barthe, C., and J.-P. Pinty (2007), Simulation of a supercellular storm using a three-dimensional mesoscale model with an explicit lightning flash scheme, *J. Geophys. Res.*, *112*, D06210, doi:10.1029/2006JD007484.

1. Introduction

[2] Lightning flashes are natural markers of the electrical activity accompanying deep convection and severe weather. They are sources of electromagnetic radiations in a wide range of frequency that make them relatively easy to detect at different spatial and temporal scales. In the past decade, various lightning detection systems have been used to monitor lightning events and their climatology. Among them, one can distinguish those operating from space like OTD (Optical Transient Detector) [*Christian et al.*, 1996], LIS (Lightning Imaging Sensor) [*Christian et al.*, 1999], FORTE (Fast Onboard Recording of Transient Events) [*Jacobson et al.*, 1999]. Other lightning detection systems operate from the ground: LASA (Los Alamos Sferic Array) [*Smith et al.*, 2002], NLDN (National Lightning Detection Network) [*Cummins et al.*, 1998] or the recent 3-D portable VLF/LF detection network [*Betz et al.*, 2004]. Moreover, the propagation of lightning is now fully trackable at storm scale. Three-dimensional detectors such as the ONERA (Office National d'Etudes et de Recherches Aérospatiales)'s Interferometric Mapper [*Laroche et al.*, 1994; *Defer et al.*, 2001] and LMA (Lightning Mapping Array) [*Rison et al.*, 1999] reveal many details on the sequence of short duration events and on the dendritic nature of lightning structures.

[3] In contrast to all these tools dedicated to observation, lightning parameterizations are far less advanced in numerical cloud models. Lightning parameterizations are indeed required to simulate long-lasting electrified storms. For instance, in the absence of a lightning scheme, the results shown by *Altaratz et al.* [2005] are restricted to the occurrence of the first lightning flash. This constitutes a severe limitation to ongoing studies of electrified storms with several tens and even hundreds of lightning flashes as simulated by *Mansell et al.* [2005] or by C. Barthe and J.-P. Pinty (Simulation of electrified storms with comparison of the charge structure and lightning efficiency, submitted to *Journal of Geophysical Research*, 2006).

[4] Lightning discharges are a key component of the electric charges cycle in thunderstorms because a charge redistribution occurs instantaneously in different part of the cloud when a lightning flash is triggered. As stressed by *MacGorman et al.* [2001], lightning limits the growth of the electric field by charge neutralization at the location of lightning channels but also unmasks and so enhances the charges of opposite polarity. Consequently, an electrification

[1]Laboratoire d'Aérologie, Toulouse, France.

0148-0227/07/2006JD007484

scheme must carefully consider a lightning parameterization at a high level of detail. In cloud resolving models, electrification schemes compute the electric charges carried by several microphysical categories of water drops and ice particles. As the scale of lightning structures is close to the spatial resolution of 3-D models (a few hundreds of meters on the vertical and 1 km on the horizontal), it is worthwhile to build a lightning scheme which explicitly considers a stepped propagation from adjacent nodes and which is able to modify locally and selectively the electric charge of individual particles. The challenging issue of lightning parameterization is to provide 3-D pictures of lightning channels with branching structures as illustrated by *Thomas et al.* [2001] from observations and as simulated by *Mansell et al.* [2002] with his stochastic dielectric breakdown model.

[5] In electrification schemes, the dynamics of the electric charges is mostly driven by the microphysical scheme [*Ziegler et al.*, 1986; *Helsdon and Farley*, 1987; *Norville et al.*, 1991; *Solomon and Baker*, 1994; *Barthe et al.*, 2005; *Altaratz et al.*, 2005]. The reason is that there are many arguments to preserve a consistency between cloud electrification schemes and cloud microphysical schemes. In the noninductive mechanism, charges are separated by elastic ice-ice collisions which are the complement of the ''efficient'' side of ice-ice collisions that leads to the growth of snow by aggregation and to the growth of graupel particles by collection of several ice particle types. The electric charges are then disseminated over the microphysical spectra by all of the microphysical processes. The charges are transported with the hydrometeors by advection, diffusion and sedimentation. As a result, the distribution of electric charges in a storm is tightly linked to the microphysical history of the storm. This microphysics-dominated state exists until a first lightning event is triggered. Lightning disrupts the unique dependence of the charge distribution on the microphysics.

[6] At the microscale, the physics of the electric charges is symmetrical since an equal amount of charge of opposite polarity is exchanged locally. However, this structure is broken at the storm scale because of the differential sedimentation rates of the charged hydrometeors. This results in the setting up of an electric field which is the leading ingredient of the lightning schemes. *MacGorman et al.* [2001] reviewed the underlying ideas of different types of lightning parameterizations and concluded that extensive flash development should be accounted ''... in regions having a weak ambient electric field but a substantial charge density.'' This new concept, studied in detail by *Mansell et al.* [2002], has been adopted and extended in the present scheme where the lightning geometry is viewed as a fractal object. Lightning channels with branching structures are explicitly determined.

[7] This paper describes an explicit lightning flash scheme which has been developed in the nonhydrostatic mesoscale model Méso-NH [*Lafore et al.*, 1998]. The scheme is thereby able to simulate a production of Lightning Nitrogen Oxides (LNO_x) [*Barthe et al.*, 2007] for atmospheric chemistry application. It also has potential application to simulate real electrified storms over complex terrain at high resolution with grid nesting. The electrification scheme [*Barthe et al.*, 2005] is briefly described in the first part of the paper, with focus on the charge conservation and on the inductive mechanism parameterization that has been recently added. The second part is dedicated to the description of the original lightning flash scheme. The lightning flash scheme is illustrated on the 3-D supercellular storm described by *Barthe et al.* [2005]. Sensitivity analyzes related to the branching scheme are performed with the supercell case and a conclusion is drawn on the properties of the lightning flash scheme.

2. Electrification Scheme in Méso-NH

2.1. Overview of Méso-NH

[8] Méso-NH is a nonhydrostatic mesoscale model that has been jointly developed by the CNRM (Centre National de la Recherche Météorologique) and by the Laboratoire d'Aérologie [*Lafore et al.*, 1998]. This multidimensional model (3-D, 2-D or 1-D versions can be easily configured) integrates an anelastic system of equations and allows for simulations of atmospheric flow ranging from the meso-alpha scale down to the microscale. Prognostic variables of the model are the three components of the wind, the dry potential temperature, several mixing ratios of the water cycle and a provision of passive scalars which is automatically generated. It contains a full inline physical package: turbulence, radiation scheme, surface processes, mixed phase microphysics, deep and shallow convection scheme, gaseous and multiphase chemistry, aerosols. Real orography and land use are initialized from files. Simulations at different scales can be done with the two-way interactive grid nesting technique [*Stein et al.*, 2000]. The code is fully vectorized and parallelized; therefore 3-D electrified cloud simulations on large domains and real case simulations can be performed. More details about Méso-NH can be found on the website (http://www.aero.obs-mip.fr/mesonh/).

2.2. Summary of the Electrification Scheme

[9] Most of the electric charges are carried by the hydrometeors revealing a strong dependence of the electrical state of the storm on the microphysics. The microphysical scheme of Méso-NH considers two categories of water drops (droplets and rain drops), three classes of ice particles (pristine ice, snow and graupel) and water vapor. The particular treatment of the water vapor is detailed in the next section. At least three ice types are necessary to cover most of the precipitating cases: pristine ice, snow/aggregates and graupel. Several categories could be distinguished for graupel depending on the degree of riming and on the growth mode as done by *Mansell et al.* [2005]. However, because of uncertainties of the charge separation mechanism, three classes of ice particles seems to be sufficient to reproduce the main characteristics of the storm.

[10] The electrification scheme has been fully described by *Barthe et al.* [2005], and it is briefly summarized herein. The electrical scheme is developed from the mixed phase microphysical scheme of the model [*Caniaux et al.*, 1994; *Pinty and Jabouille*, 1998]. The charge separation mechanisms consider noninductive processes that result from elastic collisions between particles with different degrees of riming. The noninductive charge separation parametrizations of *Takahashi* [1978], *Saunders et al.* [1991] and *Saunders and Peck* [1998] have been implemented in the

manner described in *Mansell et al.* [2005]. We do not repeat the description of these parameterizations here.

[11] The electric charges carried by each of the five hydrometeor categories are transported along the airflow and are exchanged according to the various microphysical mass transfer rates. Power law distributions of individual charges are given as a function of particle size and hydrometeor habits. This feature emphasizes the distinction between mass and charge characteristics of the hydrometeors whose electrical properties and mass transfer rates are neither proportional (mass-weighted) nor uniformly distributed with size. Disconnecting mass-size and charge-size properties of the hydrometeors brings useful degrees of freedom that are indeed absent in all the other schemes.

[12] The electric field is diagnosed at each time step after integrating the electric potential induced by a net charge density in the Poisson equation. The ground and the highest atmospheric levels are equipotential planes. Lateral boundary conditions follow *Barthe et al.* [2005].

[13] A lightning flash is triggered when the electric field locally steps over a breakeven threshold defined by *Marshall et al.* [1995]. The flash propagates in two opposite directions until the magnitude of the electric field falls below a prescribed value. A sequential fractal branching algorithm is applied to complete the extent of lightning streamers toward cloud regions where substantial charge densities are present. Charges are neutralized along the tortuous lightning path but the charge balance is considered in a different way according to the intracloud or to the cloud-to-ground character of the flash. The lightning flash scheme is fully described in section 3.

2.3. Additional Developments

2.3.1. Inductive Charging Process

[14] Additional developments have been made to the scheme originally published in *Barthe et al.* [2005]. The inductive charging mechanism is now integrated in the electrification scheme. As hydrometeors are dielectric bodies, they become polarized in a vertically pointing electric field with charges of opposite polarity accumulating at the top and at the bottom faces to form a dipole moment. When two particles collide and rebound close to their vertical axis of symmetry, charges of opposite polarity are briefly exchanged yielding a net reduction of charge in the contact zone. As a result, positive (negative) charges tend to form on big (small) size hydrometeors by this mechanism. Although the inductive mechanism cannot by itself explain the charge densities and the charge distribution usually observed in thunderstorms, it is anticipated that it is locally a nonnegligible contributor to the cloud electrification process. As mentioned by *Mansell et al.* [2005], including or excluding the inductive charging leads to a different behavior of the electrical activity. For instance, he observed that the inductive charge separation mechanism tends to enhance the positive charge zone in the low levels of a thunderstorm. Consequently, the lightning triggering altitude is lowered and the production of cloud-to-ground flashes is favored.

[15] Laboratory studies conducted by *Aufdermaur and Johnson* [1972] have shown that in the presence of an electric field stronger than a few kV m^{-1} collisions between particles would lead to significant charge exchange. Drop-drop inductive charging is not considered because most of the time the two colliding particles end up with a single bigger drop. Concerning ice-ice inductive charging, the short duration and small size of the contact zone and the low ice electrical conductivity do not allow for a substantial charge exchange when ice particles collide [*Illingworth and Caranti*, 1985]. Therefore only bouncing collisions between graupel and droplets are likely needed to be taken into account. Even if the rate of rebounding collisions is low compared to the rate of sticking collisions, the amount of charge separated is important. The inductive charging rate parameterization follows the expression given by *Ziegler et al.* [1991]:

$$\frac{\partial \rho_g(D_g)}{\partial t} = \frac{\pi}{4} E_{cg} E_r D_g^2 V(D_g) N_c \alpha \left[\frac{\pi^3}{2} D_c^2 \epsilon E_z \cos\theta - \frac{\pi^2}{6} \rho_g(D_g) \frac{D_c^2}{D_g^2} \right] \tag{1}$$

where E_{cg} is the graupel-droplets collision efficiency, E_r the rebound probability, and E_z the vertical component of the electric field. ϵ is the permittivity of air. ρ_g is the graupel charge density, D_c the cloud droplets diameter, and D_g the graupel diameter. V is the fall speed of graupel, and N_c is the number concentration of cloud droplets. The second term of the expression accounts for a preexisting charge polarity of the graupel. Assuming that grazing collisions are the most efficient ones, α is the fraction of droplets experiencing grazing trajectories, and $\cos(\theta)$ is the mean cosine collision angle. E_r, α and $\cos\ \theta$ are set to 0.1, 0.07 and 0.2, respectively, as suggested by *Ziegler et al.* [1991].

2.3.2. Electrical Variables

[16] A charge density is associated to each component of the water cycle, i.e., to each category of condensate and to the water vapor. The mass charge density (Q_x in C kg^{-1}) is the prognostic electrical state variable related to the mixing ratio r_x of species x. The governing set of prognostic equation for Q_x is

$$\frac{\partial}{\partial t}\left(\rho_{dref} Q_x\right) + \nabla \cdot \left(\rho_{dref} Q_x \mathbf{U}\right) = \rho_{dref} S_x, \tag{2}$$

where $\mathbf{U}$ is the air velocity, and S_x is the source term standing for the effects of diffusion, charging mechanisms, charge transfers and sedimentation, and charge neutralization by lightning flashes. ρ_{dref} is the fixed air density reference of the Méso-NH continuity equation.

[17] The choice of Q_x, defined as the quantity of charge on the water substance x scaled by the mass of dry air, is dictated by conservation statement of an electrical property in agreement with the flux-form advection operator of Méso-NH [*Lafore et al.*, 1998]. Total charge (in C) and mass are conserved during transport but the volume is not. As a consequence, the often used volume charge density (ρ_x in C m^{-3}) is not a suitable prognostic variable in our case. The total mass charge density is not conserved by some processes: neutralization by cloud-to-ground flashes, charged precipitating particles reaching the ground or flux of charges through a domain boundary. The mass charge density is simply related to the volume charge density by: $Q_x = \rho_x / \rho_{dref}$.

2.4. Treatment of Ions and Charge Conservation

[18] The treatment of the water vapor deserves a short discussion. During the evaporation and the sublimation of

the hydrometeors, mass is explicitly transferred from the condensate to the water vapor. The associated charge loss would correspond to the release of free ions. However, ions and the physics of ions are not yet considered in this electrical scheme, so the charge carried by the ions is symbolically attributed to that of the water vapor (we assume that ions behave more like gas molecules than solid bodies). Two reasons can explain this choice. First, as small charged hydrometeors evaporate or sublimate completely, decreasing the mixing ratio without reducing the charge carried by these hydrometeors would somehow lead to unrealistic charge/mass ratios well above the Rayleigh limit [*MacGorman and Rust*, 1998]. Second, the total electric charge must be conserved, thus, the charge associated to the transfer of mass during evaporation is stored in a "water vapor" reservoir. *Altaratz et al.* [2005] did not track the charge produced by evaporating or sublimating hydrometeors, and therefore they did not conserve the total charge. It is assumed that ion charge is not put on hydrometeors with the same sign of charge.

[19] In the microphysical scheme, a saturation adjustment is performed for the water vapor mixing ratio. In mixed phase clouds, cloud droplets and small ice crystals can coexist so fast exchanges of water vapor are necessary for a rapid return to equilibrium. A saturation vapor mixing ratio $r_{vc,i}^{sat}(T)$ is defined by a barycentric formula based on saturation over water and ice and with cloud droplet and pristine ice mixing ratios acting as weighting factors. The deposition and the condensation rates are derived from the implicit adjustment with respect to $r_{vc,i}^{sat}$. The "water vapor charge" is adjusted in proportion of the change of mixing ratio after the mass adjustment. We crudely consider that ions represented here by the "water vapor charge" are more or less sensitive to phoretic effects in the surrounding of small droplets and small crystals.

3. Lightning Flash Scheme

[20] There are two categories of lightning events that need to be reproduced in numerical models. Intracloud (IC) flashes are connecting two regions of opposite charge inside the cloud while cloud-to-ground (CG) strikes are lightning flashes that reach the ground. The latter are positive (+CG) or negative (−CG) depending on the polarity of the leader connected to the ground. A +CG flash is detected when the leader propagates in a negatively charged zone before reaching the ground. The overall effect of lightning flashes is to reduce the electrical stress inside an electrified cloud by reorganizing the electric charges and so by limiting the magnitude of the electric field. The efficiency of a lightning scheme can be checked in several aspects (frequency, location, polarity, extension). All of these characteristics of the lightning flashes are detectable and informative about the electrical activity in clouds.

[21] Moreover, it is now well established that IC flashes have a significant impact in atmospheric chemistry as they constitute an important source of nitrogen oxide (NO_x = $NO + NO_2$), an ozone precursor, in the tropical atmosphere: following *Wang et al.* [1998], an NO production rate can be estimated per unit length of discharge channel. It turns out that in addition to the frequency, the total flash length is also a key parameter to get a reliable NO_x production rate by lightning flashes [*Barthe et al.*, 2007].

3.1. Previous and Present Lightning Flash Treatments

[22] Observations of VHF emission by lightning flashes [*Shao and Krehbiel*, 1996; *Rison et al.*, 1999; *Krehbiel et al.*, 2000; *Thomas et al.*, 2001] reveal the bidirectional nature of the intracloud flashes and their large horizontal extension in one or two layers. However, a few electrification models include a realistic lightning parameterization which is consistent with these observational evidences.

[23] There are roughly two categories of lightning schemes as reviewed in *MacGorman et al.* [2001] and *Mansell et al.* [2002]. On the one hand, some bulk schemes treat the global effect of the lightning flash, i.e., a volumetric reduction of charge density excess [*Rawlins*, 1982; *Takahashi*, 1984; *Ziegler and MacGorman*, 1994]. This type of scheme is simple to implement but lacks physical insight. More realistic schemes introduce the notion of a lightning path. However, most of them only reproduce the bidirectional leader phase [*Kasemir*, 1960], a nearly vertical propagation of the flashes driven by the ambient electric field [*Helsdon et al.*, 1992] or by the net electric field [*Solomon and Baker*, 1996; *Mazur and Ruhnke*, 1998].

[24] A number of available lightning schemes focus on the vertical propagation of lightning flashes whereas branches and large horizontal extensions of the flashes were indeed observed [*MacGorman et al.*, 1981; *Shao and Krehbiel*, 1996; *Rison et al.*, 1999]. *Hager et al.* [1989] developed a deterministic lightning scheme where the channel is extended to all the points where the electric field becomes higher than a threshold. To take into account the horizontal extension of the flashes, *Helsdon et al.* [1992] included a "semivolumetric" IC parameterization in their storm electrification model [*Helsdon and Farley*, 1987] with a "neutralizing" halo zone encompassing the bidirectional leader. Allowing for flash propagation in high charge but weak electric field regions, *MacGorman et al.* [2001] were the first to draw attention to the geometrical structure of a lightning flash. Furthermore but starting from another point of view, *Niemeyer et al.* [1984] already showed that a dielectric breakdown model naturally lead to a fractal structure of discharge patterns in insulating material. Then the original algorithm of *Niemeyer et al.* [1984] was successfully adopted by *Mansell* [2000] to describe branching structures in their state-of-the-art 3-D lightning flash scheme.

[25] The dielectric breakdown approach was already mentioned by other authors to study lightning discharges. After modifications of the model of *Niemeyer et al.* [1984], *Tsonis and Elsner* [1987] were among the first to generate lightning structures qualitatively similar to those observed. *Wiesmann and Zeller* [1986] further improved their dielectric breakdown model by introducing an internal electric field to take into account the finite resistance of the ionized channel and a critical electric field to threshold the propagation. *Petrov and Petrova* [1993] used the model of *Wiesmann and Zeller* [1986] to reproduce different kinds of discharges. Numerical simulations of a stepped leader near the ground were also realized by *Kawasaki and Matsuura* [2000] using a leader progression model and the fractal concept. They succeeded in simulating the

branches of the lightning flashes. To summarize, the numerical dielectric breakdown approach has profoundly improved the traditional treatment of lightning discharges. Unfortunately, this technique suffers from an important drawback which is its heavy computational burden when solving a Laplace equation each time an elementary branch is added to the structure.

[26] The physics of lightning discharges is complex and still not well understood. Thus it seems out of reach developing a new lightning scheme in a 3-D mesoscale model solely based on true physical arguments. In the present model, attention is paid to the reproduction of the lightning flash morphology and of the major effects of the lightning flashes, i.e., the local limitation of the electric field and the local charge redistribution. The lightning scheme is made up of two different parts. First, a deterministic lightning channel develops in the manner of the bidirectional leader [*Kasemir*, 1960]. Then, branches are connected in high charge regions with a probabilistic algorithm based upon a fractal description of lightning as supported by the results of *Niemeyer et al.* [1984] and *Mansell et al.* [2002].

3.2. Electric Field Computation and Lightning Flash Triggering

[27] The electric field is a solution of the Gauss equation which involves the total volume charge density ρ_{total}:

$$\nabla \cdot \mathbf{E} = \frac{\rho_{total}}{\epsilon} \tag{3}$$

where ϵ is the permittivity of the air. The electric potential ϕ is related to the electric field by $\mathbf{E} = -\nabla\phi$. Equation (3) is solved with the parallelized elliptic pressure solver of Méso-NH, needed for the anelastic dynamics. Boundary conditions are adapted to constrain the electric field. The electric field remains orthogonal to the ground and to the highest level surfaces. It recovers a standard fair weather value on the lateral boundaries of the domain of simulation.

[28] The value of the dielectric breakdown field is about 3000 kV m^{-1} at sea level while *Marshall et al.* [1995] showed from many electric field soundings that the electric field hardly reaches more than 150 kV m^{-1} inside thunderstorms. From the detection of X-rays just before a lightning flash was triggered, *MacCarthy and Parks* [1985] concluded that relativistic electrons ($\sim$1 MeV), accelerated by the electric field, could be responsible for this X-ray emission by ionizing air molecules [*Gurevitch et al.*, 1992; *MacCarthy and Parks*, 1992]. This means that a sustained energetic electron avalanche can trigger a lightning flash for electric fields much smaller than the breakdown value. This electric field is the breakeven electric field E_{be} which is simply parameterized as a function of the altitude [*Marshall et al.*, 1995]:

$$E_{be} = \pm 167\rho_A(z) \qquad \text{with} \qquad \rho_A(z) = 1.208\exp\left(\frac{-z}{8.4}\right) \tag{4}$$

where E_{be} is in kV m^{-1} and the altitude z in km. Once the electric field is computed, a lightning flash is randomly triggered among the grid points where the electric field is higher than $0.9E_{be}$. The factor 0.9 accounts for some subgrid-scale variability of the electric field and allows for a slightly undetermined location of the lightning flash initiation as suggested by *MacGorman et al.* [2001].

3.3. Bidirectional Leader

[29] The first step of the lightning flash parameterization follows *Helsdon et al.* [1992] and the theory of *Kasemir* [1960] who considered IC lightning channels as electrically neutral conductors. Two segments of opposite polarity propagate in the direction parallel and antiparallel to the electric field. The leader propagates step by step as long as the amplitude of the electric field at the tip of the channel stays higher than a fixed propagation threshold (E_{prop} = 20 kV m^{-1}). The addition of a new segment requires the computation of angles between the electric field and the coordinate vectors. The direction of propagation of the leader is determined from these angles. The leader path follows the closest electric field line along the coordinate axes or along the diagonals. It is restricted to the forward hemisphere so the propagation is stopped when only backward propagation is possible. The bidirectional leader also stops propagating when it reaches regions of low electric field or regions where the electric field is opposed to the propagation.

[30] The criterion for propagation and termination of the leader is based on the ambient electric field instead of the true local one. We are aware that omitting for the moment the influence of the electric field induced by the lightning itself is a shortcoming [*Mazur and Ruhnke*, 1998], but it is done for the sake of simplicity and mostly to reduce the computational cost. As described previously, the electric field is computed with an elliptic solver which takes a significant computation time. Given the fact that the electric field at the tip of the leader should be recalculated each time a segment is added to the channel, a simple approach based on the ambient field is retained. It is further justified by the fact that more attention is paid to the generation of branches growing on the bidirectional leader structure.

[31] The treatment of CG flashes is more problematic. Previous tests made with the model have shown that the channel does not propagate below a critical altitude of 2 km. Many reasons can explain this deficiency. First, the electric field is possibly underestimated because of the discrete nature of the field. Indeed, the vertical grid size of the model is higher than 100 m which is larger than the physical channel width. Moreover, ions and corona effects are not considered in the model; thus the electric field below cloud is lower than the propagation threshold, and the channel can never reach the bottom of the domain. To remedy this problem, it was decided to force the leader to reach the ground when it is strictly vertically oriented in the downward direction and when the lightning tip falls below the altitude of 2 km above the ground.

3.4. Fractal Treatment of the Branches

[32] The lightning flash scheme developed by *Mansell* [2000] needs to compute the local electric field each time a new segment is added to the existing structure of the lightning. This class of scheme is grounded in the physics of electric discharges so it is suitable in the case of high resolution of the lightning channel geometry. Here a slightly different point of view is adopted to incorporate an acceptable level of detail and complexity to produce the branching

patterns. In order to limit the computation cost of the simulation, the dielectric breakdown model of *Niemeyer et al.* [1984] and the "Wild Fire" technique of *MacGorman et al.* [2001] are considered and simplified. The grid points that can be added to the channel must obey a criterion on charge density as in the work by *MacGorman et al.* [2001]. Then it is postulated that the number of branches at a distance d from the triggering point is described by the fractal law [*Niemeyer et al.*, 1984]:

$$N(d) \sim \frac{L_\chi}{L_{moy}} d^{\chi-1} \tag{5}$$

[33] The fractal dimension χ varies in the range $1 < \chi < 2$ in two dimensions and in the range $2 < \chi < 3$ in three dimensions [*Petrov and Petrova*, 1993]. The exponent χ determines the degree of branching of the lightning flashes. L_{moy} is the average length of a grid mesh, and $L\chi$ a characteristic length of the flash. d is the distance from the triggering point, expressed in number of grid points.

[34] The implementation of the fractal treatment of the branches is done as follows. The simulation domain is divided into concentric spheres (centered on the grid point where the flash is triggered) whose radii are equal to the lowest grid spacing $dl = (dx \times dy \times dz)^{1/3}$ multiplied by an integer n. The level one of branching is first performed. The first level corresponds to branches that are directly linked to the bidirectional leader. When a branch is attached to a first level branch, its level of branching is two, and so on. The branches linking the bidirectional leader and the contiguous nodes with $\rho > \rho_{excess}$ are explored. The probability of branching is inversely proportional to the number of possible bonds. Even if the probability does not depend explicitly on the strength of the electric field as in the work by *Mansell et al.* [2002], the technique is able to simulate the growth of a lightning structure and a qualitative screening effect. This means that open sites, like those at the tips of the branches, are favored against interior sites which are embedded in the branched structure.

[35] The total cloud is examined using the sphere of increasing radius $n \times dl$ starting from $n = 1$. For each sphere, the number of preexisting branches is calculated together with the maximum number of branches at this distance (equation (5)). If the number of preexisting branches at distance d is equal or larger than the maximum number of branches, $N(d)$, no more segments are added. In the opposite case, new bonds are added to the flash starting from the grid points having the highest probability of connection and selecting at random those having an equal probability [*Mansell*, 2000]. Once the whole bidirectional leader structure is explored for the first level of branching, the procedure is applied to the second level of branching with roots on the branches of level one, and so on until no more branching is possible.

3.5. Neutralization

[36] Because of the very high temperatures inside the lightning channel, air molecules become ionized. The induced free ions diffuse away from the channel and partially neutralize the charged hydrometeors of opposite polarity. The net result is that lightning flashes neutralize an equal amount of positive and negative charge and reduce the electric field in the cloud. Thus, once the entire lightning channel is obtained, the electric charges are redistributed along the path. The parameterization of the neutralization process is adapted from the work of *Ziegler and MacGorman* [1994] and *MacGorman et al.* [2001]. The charge is neutralized for the channel grid points (i, j, k) where the charge density is higher than a given threshold ρ_{excess}:

$$\begin{cases} \delta\rho(i,j,k) = \pm(|\rho(i,j,k)| - \rho_{excess}) & \text{if } |\rho(i,j,k)| > \rho_{excess} \\ \delta\rho(i,j,k) = 0 & \text{otherwise,} \end{cases} \tag{6}$$

where $\rho(i, j, k)$ is the total electric charge along the lightning flash. In the case of IC flashes, the total charge neutrality of the channel must be respected [*Kasemir*, 1960]. The total charge of the flash is summed algebraically, and if non zero, the residual is distributed on each grid point of the channel. The correction applied to each grid point of an IC flash is then:

$$\delta\rho_{neut} = \sum_{i,j,k} \delta\rho(i,j,k) \times \frac{1}{N} \tag{7}$$

where N is the number of grid points reached by the lightning flash. Since the ions are not explicitly treated in the model, the ions released by lightning flashes are directly attached to the different hydrometeor categories. It is assumed that each hydrometeor category receives the quantity of charge in proportion to the hydrometeor surface area σ:

$$\frac{d\rho_x(i,j,k)}{dt} = [\delta\rho(i,j,k) - \delta\rho_{neut}] \frac{\sigma_x(i,j,k)}{\sum_l \sigma_l(i,j,k)} \tag{8}$$

The quantity of charge neutralized on each grid point depends on the preexisting charge at this point. In the case of CG flashes, the charge neutrality constraint (equation (6)) no longer applies.

4. Storm Initiation and Evolution

4.1. Initialization

[37] The supercellular storm described by *Barthe et al.* [2005] has been chosen to illustrate the lightning flash scheme efficiency. The simulation lasts 80 min, and the domain is 40 km $\times$ 40 km $\times$ 15 km with a resolution of 1 km on the horizontal and 500 m on the vertical. Convection is initiated by a warm bubble located in the planetary boundary layer, at the southwestern corner of the domain. The initial sounding comes from *Klemp and Wilhelmson* [1978]. The idealized hodograph is characterized by a vertical shear with a low level veering and an upper level wind constant in speed and direction (southwestern flow).

[38] The parameterization of *Saunders et al.* [1991] is used to describe the noninductive process. This parameterization has been modified at low liquid water content as suggested by *Helsdon et al.* [2001]. The inductive mechanism is considered. Open boundary conditions are applied in both x and y directions. A numerical absorbent is placed in the upper levels to damp vertically propagating gravity waves. Advection of the moist and electrical variables is

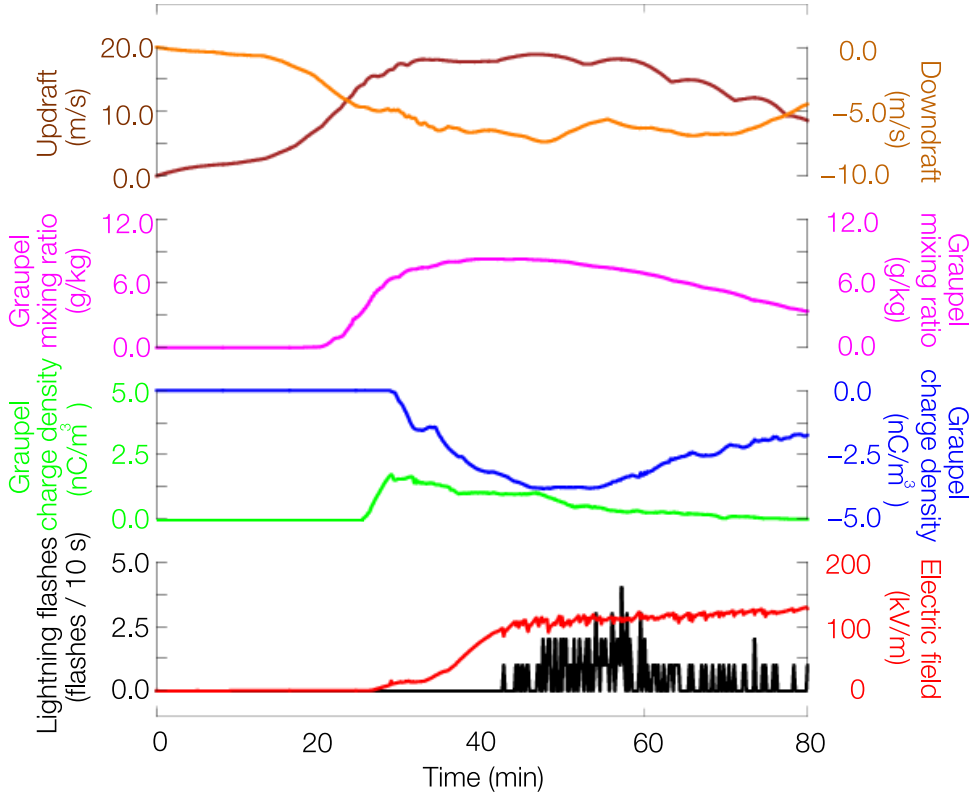

Figure 1. Temporal evolution of different parameters. From the top to the bottom, the plotted parameters are the maximum positive (maroon curve) and negative (orange curve) vertical velocities (in m s^{-1}), the maximum graupel mixing ratio (pink curve) (in g kg^{-1}), the maximum positive (green curve) and negative (blue curve) graupel charge densities (in nC m^{-3}), the maximum electric field (red curve) (in kV m^{-1}), and the lightning flash frequency (black curve) (in number of flashes per 10 s).

done with the MPDATA (Multidimensional Positive Definite Advection Transport Algorithm) scheme. The branching parameters χ and L_χ are set to 2.5 and 500 m respectively.

4.2. Storm Evolution

[39] The temporal evolution of the peak value of some selected parameters is depicted in Figure 1. Starting from the top, the updraft speed reaches a maximum value of 18 m s^{-1} after 30 min. Then it gradually decreases as the storm dissipates. The downdraft velocity follows a symmetrical evolution and attains −7 m s^{-1} during the mature stage. The supercell is not very intense since the vertical velocity in storms often exceeds 30 m s^{-1}. It results in a weak vertical extension of the cloud with a cloud top less than 10 km altitude. The next curve of Figure 1 shows the maximum value of the graupel mixing ratio which stays below the 9 g kg^{-1} level that is reached after 40 min of simulation. There is a short delay of approximately 5–10 min between the updraft and the graupel signals as the buildup of elaborated microphysical species such as the graupel is necessarily lagged because of inherent microphysical time scales.

[40] The electric field and the total charge densities (positive and negative values) are the next analyzed variables. They are a good indicator of the lightning flash scheme efficiency and of the microphysical state of the storm. Lightning flashes are triggered among the grid points where the electric field peaks above E_{be} (equation (4)). Neutralizing the charges tends to reduce the total charge density and by extension to limit the growth of the electric field. In Figure 1, the early generation of the charges is roughly delayed by 10 min with the very first production of graupel-like, rimed ice particles that have a prominent role in the cloud electrification processes. This is explained by the sedimentation timescales of the different particles that lead to a macroscopic charge separation at the cloud scale. The maximum graupel charge density turns around ±3 nC m^{-3} on average. The traces are not symmetrical. The amplitude of the maximum charge density decreases with the storm activity.

[41] The amplitude of the maximum ambient electric field is plotted at the bottom of Figure 1. The signal clearly never exceeds 200 kV m^{-1} indicating a satisfying efficiency of the complex lightning scheme. Relatively high frequency but small fluctuations are also present on the trace. They are indicative of the lightning flash activity. The growth of the maximum electric field is still visible even during the mature stage of the storm. The storm is developing electrically at lower altitudes, where the triggering threshold is higher.

[42] Lightning flash frequency is also plotted in the bottom plot of Figure 1. Lightning flashes are triggered 15 minutes after the electric field has started to increase. The maximum electrical activity takes place after one hour of simulation, and the lightning flash frequency is about

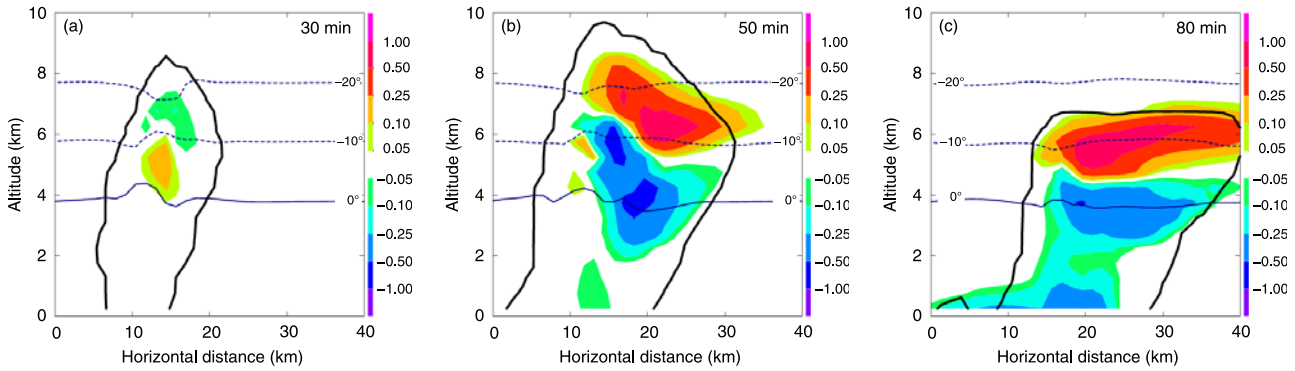

Figure 2. Vertical cross sections of the total charge density (colored areas) at (a) 30 min, (b) 50 min, and (c) 80 min. The horizontal lines represent the 0°C, −10°C, and −20°C isotherms. The black curve shows the cloud boundary.

4 flashes every 10 s. Then the flash frequency decreases in relation to the dissipation of the electric charge.

[43] Figure 2 shows a series of vertical cross sections of the total charge density taken at different stages of the supercell life cycle. All the vertical cross sections are taken along the upper level wind and go through the maximum updraft core. At 30 min, a positive charge region is located below a negative charge region. In this first stage, the positive noninductive charging of graupel is dominant: graupels gain a positive charge and ice crystals a negative charge. Because of different sedimentation rates between ice crystals and graupels, an inverted dipole shows up. Positive values reach 0.1 nC m^{-3}, and negative values are only 0.05 nC m^{-3}. No lightning flashes are triggered during this stage of the storm because of the low charge density.

[44] Twenty minutes later, the inverted dipole no longer exists. A positive charge extends in the upper part of the cloud, between the −10°C and the −20°C isotherms while a negative charge region is located below the −10°C isotherm. The values of the total charge density have increased to reach ±0.8 nC m^{-3} in both the positive and the negative regions. Most of the noninductive charging mechanism of the graupel has switched to negative which results in a direct dipole. The electrical structure combines the electrical state of the hydrometeors and the dynamical properties of the particles and of the flow. The transition from an inverted dipole to a direct dipole when using the *Saunders et al.* [1991] parameterization has already been simulated by *Helsdon et al.* [2001] and *Mansell et al.* [2005]. In the vigorous part of the updraft where supercooled droplets coexist with graupel, the inductive charging is active and increases the charge of graupel. As a result, the lower pole of our simulated storm is reinforced as noted by *Mansell et al.* [2005].

[45] At 80 min, the storm enters into the dissipation stage. The boundary between the two opposite charge regions has collapsed to the altitude of 4–5 km, while it was around 6 km 30 min earlier.

[46] Moreover, the shape of the charge regions has changed. Both positive and negative charge regions spread out when the storm starts to dissipate.

[47] Below the freezing level of the downdraft, the graupels melt into raindrops which results in negative precipitation. The total charge density decreases because of a sustained lightning flash activity and because of a less efficient rate of separation in the upper levels. The positively charged anvil is crossing the horizontal domain boundary.

5. Efficiency of the Branching Scheme

[48] The treatment of the lightning flashes is novel and it is the most complex part of the complete cloud electrification scheme. It raises the question of the usefulness of such a detailed scheme. This section illustrates this point through sensitivity experiments which are analyzed.

5.1. Illustration of an IC Flash

[49] Figure 3 shows a 3-D perspective of the volumic surface wrapping a single lightning flash. In other words, it corresponds to the influence zone of a lightning flash where hydrometeor charges are neutralized after this flash event.

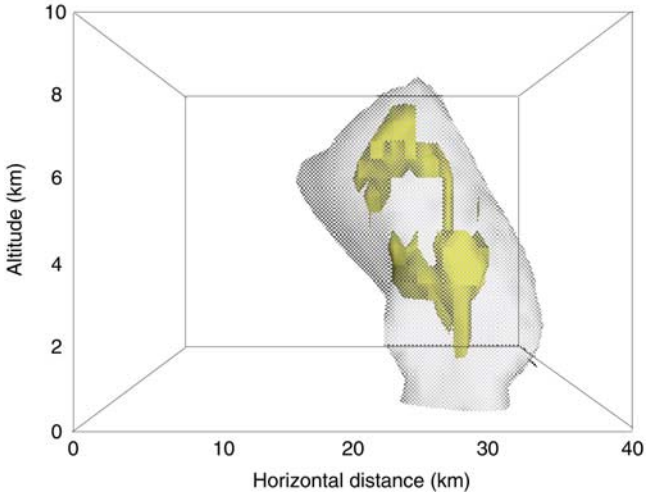

Figure 3. Surface over the region of a lightning flash (yellow surface) triggered at 2984 s. It represents the volume affected by an individual lightning flash with the branching scheme. The initiation altitude of this flash is 5500 m. The lightning flash is viewed from the west side of the domain. The overlying light gray surface shows the cloud boundary.

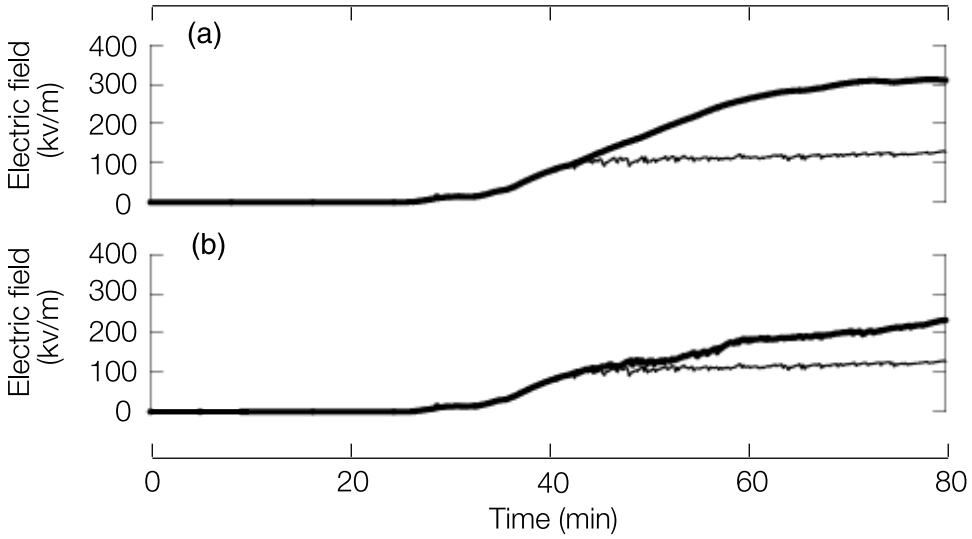

Figure 4. Temporal evolution of the maximum electric field (in kV m^{-1}). (a)Maximum electric field when the lightning flash scheme is not used (thick line). (b) Represents the maximum electric field when the branching scheme is not used (thick line). In both Figures 4a and 4b, the thin line shows the maximum electric field when the complete lightning flash scheme is taken into account.

The flash was triggered at 5500 m altitude during the mature stage. The lightning flash exhibits a two-layer horizontal structure. The upper layer is located around 7 km altitude, while the lower layer is centered around 4 km. The upper and lower levels of the flash are associated to the positive and to the negative charge regions, respectively. This flash structure looks like observed ones reported by several investigators such as *Shao and Krehbiel* [1996] and *Rison et al.* [1999]. *Mansell et al.* [2002] simulated intracloud and cloud-to-ground discharges with their 3-D branched lightning flash model and showed that an IC flash often exhibits a ''bilevel'' horizontal structure. The difference of altitude between the IC flashes simulated by Méso-NH and those of *Mansell et al.* [2002] is related to the different altitudes of the charge regions. In the work by *Mansell et al.* [2005], the upper positive and the main negative charge regions of their multicell are centered at 10 km and 8 km altitude, respectively. The storm simulated here comes from a different sounding. It produces a positive charge layer at 7 km altitude and a negative charge region at 4 km altitude. This difference of charge location is due to weaker vertical extension of the storm simulated by Méso-NH. The spatial extension of this IC flash is also in agreement with observations [*Shao and Krehbiel*, 1996; *Rison et al.*, 1999].

5.2. Sensitivity to the Lightning Scheme

[50] Two additional experiments are realized to examine the sensitivity of the electric field to the branching scheme. A first experiment is made without lightning flash while in the second experiment, only the bidirectional leader stage is activated.

[51] Figure 4 illustrates the efficiency of the lightning scheme to physically bound the growth of the electric field. Figure 4a corresponds to the first experiment. It shows that the maximum recorded value of E can nearly reach 300 kV m^{-1}. This is three times more than the same simulation run with the full lightning scheme. In the absence of lightning discharges, the evolution of the electric field shows a smooth ascending curve. Figure 4b is related to a simulation that ignores the branching stage. In this case, E peaks around 235 kV m^{-1} which is larger than the value of the breakeven field [*Marshall et al.*, 1995] despite a strong increase of the number of the flashes. In the simulation with the complete lightning flash scheme, 118 flashes are triggered while the number of lightning flashes in the simulation without branching stage is 427, i.e., 3.5 times more. This demonstrates that the full lightning scheme must be considered because it clearly provides a better limitation to the growth of the electric field.

[52] The effect of the lightning scheme on the total electric charges is the purpose of Figure 5. The cross section is selected the same as in Figure 2. The total charge density differences have been plotted after 80 min of simulation. The difference means that the resulting field of the standard simulation is substracted from the field without the lightning flash scheme (Figure 5a) and from the field without the branching scheme (Figure 5b). In the absence of lightning discharge or with a truncated scheme (no branch generation), the charge density differences is about two times more than if the complete lightning flash scheme is considered. The two charge centers are amplified meaning that no charge is presently neutralized (Figure 5a) or that only a small amount of charge is neutralized (Figure 5b) in the second experiment. This sensitivity study illustrates how a degraded representation of the lightning flashes may induce subtle charge redistributions.

[53] In the absence of the branching algorithm, an average of 0.85 C of charge of each polarity is deposited by an individual flash. This value increases to 7.68 C when the complete lightning flash scheme is used. This difference is related to the lowest number of segments in the absence of the branching scheme. In both cases, the charge neutralized at each point of the channel is about 0.12 nC m^{-3}. A mean bidirectional leader is composed of 13 segments per flash in average while a branched flash has 128 segments. Thus the

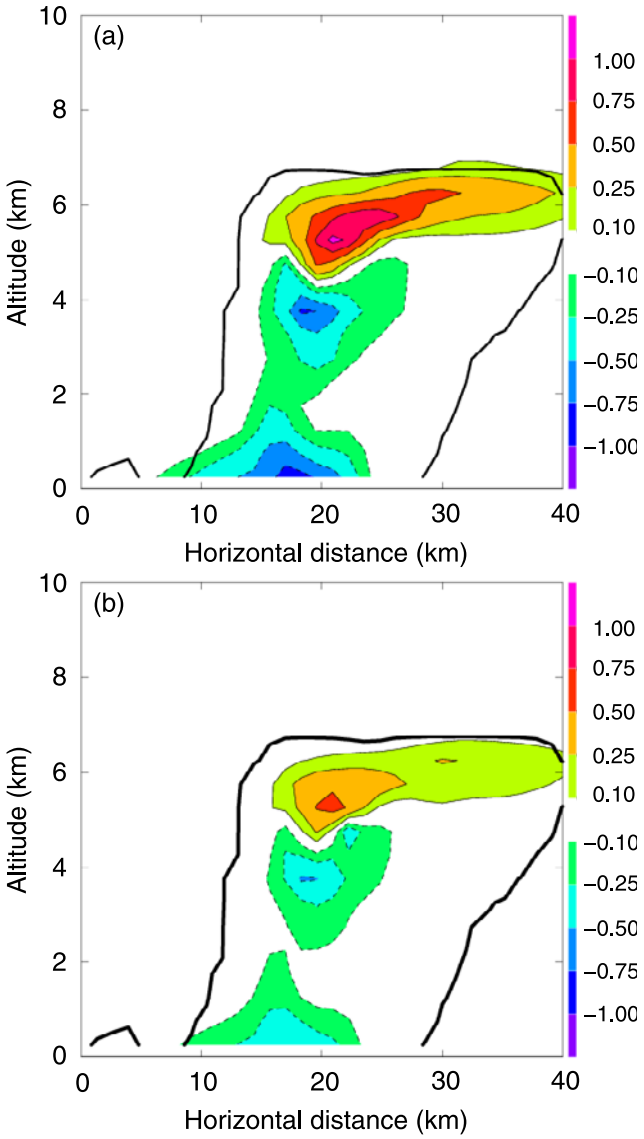

Figure 5. Vertical cross sections of the difference of total charge density (colored areas) at 80 min between (a) the simulation with and without the complete lightning scheme and (b) the simulation with and without the branching algorithm. The black curve shows the cloud boundary.

total length of an individual flash is about 140 km when the complete flash scheme is used. Adding the branching algorithm leads to an increase of charge neutralized and total flash length by a factor 10.

5.3. Sensitivity Analysis of the Fractal Parameters

[54] Simulations have been done for different values of the fractal parameters introduced in equation (5) where χ is the fractal dimension of lightning flashes and L_χ, a flash segment length scale. Sensitivity tests have been performed by varying χ and L_χ, independently. The results are reported in Table 1 where a quick look indicates that a big change in χ and in L_χ still limit the electric field ($E_{max} \sim 130-140$ kV m^{-1}) to a breakeven value in any cases.

[55] The influence of the fractal dimension on various electrical parameters is first investigated. χ is set to 2.2, 2.5 and 2.8 and L_χ is kept to a value of 500 m. It is expected that for an individual flash, an increase of χ will produce more branches in the structure of the flash. As a result, increasing the flash length leads to more charges to be neutralized per flash and finally less lightning flashes during the simulation. Simulation results reported in Table 1 are in agreement with such an explanation. An increase in χ enhances the mean number of segments per flash, and decreases the number of lightning flash. The average level of branching (~7.5) is unaffected by variations of χ meaning that the flashes are allowed to propagate in a similar volume of cloud of high charge density.

[56] The influence of L_χ on lightning flash parameters is now studied while keeping $\chi = 2.5$. For an individual flash, an increase of L_χ has the same effect as increasing the fractal dimension. Looking at Table 1, it is evident that an increase in L_χ produces results broadly comparable to those produced with an enhancement of χ. However an excessive sensitivity appears when taking $L_\chi = 200$ m. The average number of segments per flash is 38 while it is close to values around 100 and above in the other cases. Furthermore, the average number of branching is 3.1 while it is around 7.5 for all the other settings of χ and L_χ. A low value of L_χ causes a low L_χ/L_{moy} ratio. Therefore the maximum allowed number of branches at a low distance from the triggering point is zero. When the distance increases, the maximum number of branches is slightly enhanced, but not enough to allow for a good flash expansion. As a few charges are neutralized by individual flashes, three times more flashes are triggered to compensate their inefficiency to neutralize the excess of charges. This shows that the L_χ value is the most critical one that should not be set to a value lower than the vertical resolution of the simulation domain.

[57] This test shows that the mean flash length and the number of individual flashes are sensitive to the fractal parameters while the total flash length is much less (an average of 15,000 segments are processed in each simulation). Excluding the 2nd row of Table 1, the flash length varies by a factor 2.0 while the number of lightning flashes ranges from 90 to 146. The branching algorithm is robust because a balance phenomenon takes place: when the fractal parameters do not allow highly branched structures, meaning efficient neutralizing flashes, the number of triggered flashes increases. The compensation between flash length and number of flashes always succeeds in limiting the electric field to breakeven values. A recommendation of

Table 1. Table of Sensitivity Tests Concerning the Fractal Dimension of Lightning Flashes[a]

χ	L_χ, m	E_{max}, kV m^{-1}	Number of Flashes	Average Number of Segments per Flash	Average Level of Branching
2.2	500	131	146	89	7.4
2.5	200	138	313	38	3.1
2.5	500	130	118	128	7.6
2.5	1000	130	90	174	7.5
2.8	500	130	92	170	7.4

[a] χ is the fractal dimension of the flash and L_χ the characteristic length of the lightning flash. E_{max} is the maximum electric field reached during the simulation (in kV m^{-1}).

the study is to adopt the following rules: $2.5 < \chi < 2.8$ and $500\ \text{m} < L\chi < 1000\ \text{m}$. These ranges of values present the lowest sensitivity to the tuning of the couple of flash parameters.

6. Conclusion

[58] The main purpose of this work is to describe and to evaluate the properties and the bulk sensitivity of an original lightning flash scheme for use in a mesoscale model at high horizontal resolution, typically aimed at the one kilometer scale. The scheme is part of an extensive cloud electrification scheme that comprises a set of prognostic equations of the electric charges, the calculation of electric field (in generalized coordinates so it is applicable to nonflat terrain) and an advanced representation of the lightning flashes. The study reviews some recent improvements brought to *Barthe et al.* [2005] and illustrates the global behavior of the lightning scheme at storm scale.

[59] The lightning flash parameterization is composed of two parts. A lightning flash is triggered when the ambient electric field crosses the breakeven threshold. The flash first propagates as a bidirectional leader which is mostly vertically oriented along the electric field line. This is the deterministic step of the propagation scheme which is common to many schemes. The original part of the present scheme comes from the superimposed fractal representation of the lightning discharge. The purpose of it is to capture the global morphology of the flashes, i.e., to reproduce a realistic filamentary branched structure with a multilevel horizontal extension as observed. Determining the path of the lightning flash is important for the charge neutralization as well as for the frequency, the location and the total length of the flashes. The scheme is inspired by the dielectric breakdown models of *Niemeyer et al.* [1984] and *Mansell* [2000] that generate the topological characteristics of a fractal geometry. The present scheme sticks with this approach but with a helpful and necessary simplification in the parameterization of the branching probabilities to save computing resources. The scheme is iterative and the code is parallel. The buildup of the fractal structure is spatially constrained to regions where the density of the charges is high enough. The electric charges are neutralized along the whole lightning path which includes the bidirectional leader and the branches. No neutralization balance is performed for CG flashes. The probabilistic part of the lightning flash scheme, the branching algorithm, is a substitute for the still unknown physical conditions of the random progression of natural flashes in real clouds.

[60] The whole electrification scheme is tested in the 3-D mesoscale model Méso-NH to outline the electrical history of an idealized deep convection event. Results show that the scheme works satisfactorily and can bring an original electrical signature to the successive phases of the storm. The scheme used with the *Saunders et al.* [1991] parameterization of noninductive charge separation mechanism produces an inverted dipole structure that evolves into a direct dipole as already simulated by *Helsdon et al.* [2001] and *Mansell et al.* [2005] in other case studies. The lightning scheme shows its capacity to regulate the electric charge of the storm as a result of the intense and continuous noninductive (and inductive but with a lesser impact) charging processes in the updraft.

[61] The next application of the electrification scheme will address the charging mechanisms in several idealized convective cases but it is worth mentioning that the scheme already contains all the ingredients to simulate electrified clouds in real meteorological situations.

Notation

ρ_g	charge density on graupel (C m^{-3}).
D_g	graupel diameter (m).
D_c	pristine ice diameter (m).
E_{cg}	graupel-droplets collision efficiency.
E_r	rebound probability.
V	terminal fall velocity of graupel (m s^{-1}).
N_c	number concentration of cloud droplets (L^{-1}).
α	number of cloud droplets experiencing grazing collisions.
θ	collision angle.
ϵ	permittivity of air ($\epsilon = 8.8592 \times 10^{-12}$ F m^{-1}).
E_z	vertical component of the electric field (V m^{-1}).
Q_x	mass charge density of species x (C kg^{-1}).
ρ_{dref}	reference density of dry air (kg m^{-3}).
ρ_x	volume charge density of species x (C m^{-3}).
$\mathbf{U}$	air velocity (m s^{-1}).
$r_{vc,i}^{sat}$	saturation vapor mixing ratio (kg kg^{-1}).
$\mathbf{E}$	electric field vector (V m^{-1}).
ρ_{total}	total volume charge density (C m^{-3}).
ϕ	electric potential (V).
E_{be}	breakeven electric field (kV m^{-1}).
ρ_A	air density (kg m^{-3}).
z	altitude (m).
E_{prop}	electric field threshold for leader propagation (20 kV m^{-1}).
$N(d)$	number of branches at a distance d from the triggering point.
d	distance from the triggering point.
L_χ	characteristic length of the flash (m).
L_{moy}	average length of a grid mesh (m).
χ	fractal dimension of the flash.
ρ_{excess}	threshold for branching and charge neutralization (0.3 nC m^{-3}).
ρ_{neut}	correction of charge for IC neutralization (nC m^{-3}).
N	number of grid points reached by the lightning flash.
σ	total surface area of hydrometeors.

[62] **Acknowledgments.** The first author C. B. thanks D. MacGorman and T. Mansell of the National Severe Storm Laboratory (NOAA), Norman, Oklahoma, for their hospitality and for the useful discussions during her short stay in the United States while completing her Ph.D. diploma. The authors also thank F. Roux of Laboratoire d'Aérologie and University "Paul Sabatier" of Toulouse (France) for their encouragements and for their financial support (ATUPS funding). Gilles Molinié from LTHE in Grenoble (France) is warmly acknowledged for his precious help in developing the lightning scheme. Juan Escobar and Didier Gazen (both at LA) are thanked for their assistance in parallelizing the lightning scheme.

References

Altaratz, O., T. Reisin, and Z. Levin (2005), Simulation of the electrification of winter thunderclouds using the three-dimensional Regional Atmospheric Modeling System (RAMS) model: Single cloud simulations, *J. Geophys. Res.*, *110*, D20205, doi:10.1029/2004JD005616.

Aufdermaur, A. N., and D. A. Johnson (1972), Charge separation due to riming in an electric field, *Q. J. R. Meteorol. Soc.*, *98*, 369–382.

Barthe, C., G. Molinié, and J.-P. Pinty (2005), Description and first results of an explicit electrical scheme in a 3D cloud resolving model, *Atmos. Res.*, *76*, 95–113.

Barthe, C., J.-P. Pinty, and C. Mari (2007), Lightning-produced NO_x in an explicit electrical scheme tested in a Stratosphere-Troposphere Experiment: Radiation, Aerosols, and Ozone case study, *J. Geophys. Res.*, *112*, D04302, doi:10.1029/2006JD007402.

Betz, H.-D., K. Schmidt, P. Oettinger, and M. Wirz (2004), Lightning detection with 3-D discrimination of intracloud and cloud-to-ground discharges, *Geophys. Res. Lett.*, *31*, L11108, doi:10.1029/2004GL019821.

Caniaux, G., J.-L. Redelsperger, and J.-P. Lafore (1994), A numerical study of the stratiform region of a fast-moving squall line. Part I: General description and water and heat budgets, *J. Atmos. Sci.*, *51*, 2046–2074.

Christian, H. J., K. T. Driscoll, S. J. Goodman, R. J. Blakeslee, D. A. Mach, and D. E. Buechler (1996), The Optical Transient Detector (OTD), paper presented at 10th International Conference on Atmospheric Electricity, Int. Comm. on Atmos. Electr., Osaka, Japan.

Christian, H. J., et al. (1999), The Lightning Imaging Sensor (LIS), paper presented at 11th International Conference on Atmospheric Electricity, Int. Comm. on Atmos. Electr., Guntersville, Ala.

Cummins, K. L., M. J. Murphy, E. A. Bardo, W. L. Hiscox, R. B. Pyle, and A. E. Pifer (1998), A combined TOA/MDF technology upgrade of the U. S. National Detection Network, *J. Geophys. Res.*, *103*, 9035–9044.

Defer, E., P. Blanchet, C. Théry, P. Laroche, J. E. Dye, M. Venticinque, and K. L. Cummins (2001), Lightning activity for the July 10, 1996, storm during the Stratosphere-Troposphere Experiment: Radiation, Aerosol, and Ozone-A (STERAO-A) experiment, *J. Geophys. Res.*, *106*(D10), 10,151–10,172.

Gurevitch, A. V., G. M. Milikh, and R. Roussel-Dupré (1992), Runaway electron mechanism of air breakdown and preconditioning during a thunderstorm, *Phys. Lett. A*, *165*, 463–468.

Hager, W. W., J. S. Nisbet, J. R. Kasha, and W.-C. Shann (1989), Simulations of electric fields within a thunderstorm, *J. Atmos. Sci.*, *46*, 3542–3558.

Helsdon, J. H., and R. D. Farley (1987), A numerical modeling study of a Montana thunderstorm: 2. Model results versus observations involving electrical aspects, *J. Geophys. Res.*, *92*, 5661–5675.

Helsdon, J. H., G. Wu, and R. D. Farley (1992), An intracloud lightning parameterization scheme for a storm electrification model, *J. Geophys. Res.*, *97*, 5865–5884.

Helsdon, J. H., W. A. Wojcik, and R. D. Farley (2001), An examination of thunderstorm-charging mechanism using a two-dimensional storm electrification model, *J. Geophys. Res.*, *106*, 1165–1192.

Illingworth, A. J., and J. M. Caranti (1985), Ice conductivity restraints on the inductive theory of thunderstorm electrification, *J. Geophys. Res.*, *90*, 6033–6039.

Jacobson, A. R., S. O. Knox, R. Franz, and D. C. Enemark (1999), FORTE observations of lightning radio-frequency signatures: Capabilities and basic results, *Radio Sci.*, *34*(2), 337–354.

Kasemir, H. W. (1960), A contribution to the electrostatic theory of a lightning discharge, *J. Geophys. Res.*, *65*, 1873–1878.

Kawasaki, Z., and K. Matsuura (2000), Does a lightning channel show a fractal?, *Appl. Energy*, *67*, 147–158.

Klemp, J. B., and R. B. Wilhelmson (1978), The simulation of three-dimensional convective storm dynamics, *J. Atmos. Sci.*, *35*, 1070–1096.

Krehbiel, P., R. J. Thomas, W. Rison, T. Hamlin, J. Harlin, and M. Davis (2000), GPS-based mapping system reveals lightning inside storms, *Eos Trans. AGU*, *81*(3), 21.

Lafore, J., et al. (1998), The Meso-NH atmospheric simulation system. Part I: Adiabatic formulation and control simulations, *Ann. Geophys.*, *16*, 90–109.

Laroche, P., A. Bondiou, P. Blanchet, and J. Pigère (1994), 3D VHF mapping of lightning discharge within a storm, paper presented at Foudre et Montagne 94, SEE/CAF, Chamonix, France.

MacCarthy, M. P., and G. K. Parks (1985), Further observations of X rays inside thunderstorms, *Geophys. Res. Lett.*, *12*, 393–396.

MacCarthy, M. P., and G. K. Parks (1992), On the modulation of X rays fluxes in thunderstorms, *J. Geophys. Res.*, *97*, 5857–5864.

MacGorman, D. R., and W. D. Rust (1998), *The Electrical Nature of Storms*, Oxford Univ. Press, New York.

MacGorman, D. R., A. A. Few, and T. L. Teer (1981), Layered lightning activity, *J. Geophys. Res.*, *86*, 9900–9910.

MacGorman, D. R., J. M. Straka, and C. L. Ziegler (2001), A lightning parameterization for numerical cloud model, *J. Appl. Meteorol.*, *40*, 459–478.

Mansell, E. R. (2000), Electrification and lightning in simulated supercell and non-supercell thunderstorms, Ph.D. thesis, Univ. of Okla., Norman.

Mansell, E. R., D. R. MacGorman, C. L. Ziegler, and J. M. Straka (2002), Simulated three-dimensional branched lightning in a numerical thunderstorm model, *J. Geophys. Res.*, *107*(D9), 4075, doi:10.1029/2000JD000244.

Mansell, E., D. R. MacGorman, C. L. Ziegler, and J. M. Straka (2005), Charge structure and lightning sensitivity in a simulated multicell thunderstorm, *J. Geophys. Res.*, *110*, D12101, doi:10.1029/2004JD005287.

Marshall, T. C., M. P. MacCarthy, and W. D. Rust (1995), Electric field magnitudes and lightning initiation in thunderstorms, *J. Geophys. Res.*, *100*, 7097–7103.

Mazur, V., and L. H. Ruhnke (1998), Model of electric charges in thunderstorms and associated lightning, *J. Geophys. Res.*, *103*, 23,299–23,308.

Niemeyer, L., L. Pietronero, and H. J. Wiesmann (1984), Fractal dimension of dielectric breakdown, *Phys. Rev. Lett.*, *52*, 1033–1036.

Norville, K., M. Baker, and J. Latham (1991), A numerical study of thunderstorm electrification: Model development and case study, *J. Geophys. Res.*, *96*, 7463–7481.

Petrov, N. I., and G. N. Petrova (1993), Physical mechanisms for intracloud lightning discharges, *Tech. Phys.*, *44*, 472–475.

Pinty, J.-P., and P. Jabouille (1998), A mixed-phase cloud parameterization for use in mesoscale non hydrostatic model: Simulations of a squall line and of orographic precipitations, paper presented at Conference of Cloud Physics, Am. Meteorol. Soc., Everett, Wash.

Rawlins, F. (1982), A numerical study of thunderstorm electrification using a three-dimensional model incorporating the ice phase, *Q. J. R. Meteorol. Soc.*, *108*, 779–800.

Rison, W., R. J. Thomas, P. R. Krehbiel, T. Hamlin, and J. Harlin (1999), A GPS-based three-dimensional lightning mapping system: Initial observations in central New Mexico, *Geophys. Res. Lett.*, *26*, 3573–3576.

Saunders, C. P. R., and S. L. Peck (1998), Laboratory studies of the influence of the rime accretion rate on charge transfer during crystal/graupel collisions, *J. Geophys. Res.*, *103*, 13,949–13,956.

Saunders, C. P. R., W. D. Keith, and R. P. Mitzeva (1991), The effect of liquid water on thunderstorm charging, *J. Geophys. Res.*, *96*, 11,007–11,017.

Shao, X. M., and P. R. Krehbiel (1996), The spatial and temporal development of intracloud lightning, *J. Geophys. Res.*, *101*, 26,641–26,668.

Smith, D. A., K. B. Eack, J. Harlin, M. J. Heavner, A. R. Jacobson, R. S. Massey, X. M. Shao, and K. C. Wiens (2002), The Los Alamos Sferic Array: A research tool for lightning investigations, *J. Geophys. Res.*, *107*(D13), 4183, doi:10.1029/2001JD000502.

Solomon, R., and M. Baker (1994), Electrification of New Mexico thunderstorms, *Mon. Weather Rev.*, *122*, 1878–1886.

Solomon, R., and M. Baker (1996), A one-dimensional lightning parametrization, *J. Geophys. Res.*, *101*(D10), 14,983–14,990.

Stein, J., E. Richard, J.-P. Lafore, J.-P. Pinty, N. Asencio, and S. Cosma (2000), High resolution non-hydrostatic simulations of flash-floods episodes with grid-nesting and ice-phase parameterization, *Meteorol. Atmos. Phys.*, *72*, 101–110.

Takahashi, T. (1978), Riming electrification as a charge generation mechanism in thunderstorms, *J. Atmos. Sci.*, *35*, 1536–1548.

Takahashi, T. (1984), Thunderstorm electrification—A numerical study, *J. Atmos. Sci.*, *41*, 2541–2558.

Thomas, R. J., P. R. Krehbiel, W. Rison, T. Hamlin, J. Harlin, and D. Shown (2001), Observations of VHF source powers radiated by lightning, *Geophys. Res. Lett.*, *28*, 143–146.

Tsonis, A. A., and J. B. Elsner (1987), Fractal characterization and simulation of lightning, *Beitr. Phys. Atmos.*, *60*, 187–192.

Wang, Y., D. J. Jacob, and J. A. Logan (1998), Global simulation of tropospheric O_3-NO_x-hydrocarbon chemistry: 1. Model formulation, *J. Geophys. Res.*, *103*, 10,713–10,725.

Wiesmann, H. J., and H. R. Zeller (1986), A fractal model of dielectric breakdown and prebreakdown in solid dielectrics, *J. Appl. Phys.*, *60*, 1770–1773.

Ziegler, C. L., and D. R. MacGorman (1994), Observed lightning morphology relative to modeled space charge and electric field distributions in a tornadic storm, *J. Atmos. Sci.*, *51*, 833–851.

Ziegler, C. L., P. S. Ray, and D. R. MacGorman (1986), Relations of kinematics, microphysics and electrification in an isolated mountain thunderstorm, *J. Atmos. Sci.*, *43*, 2098–2115.

Ziegler, C. L., D. R. MacGorman, J. E. Dye, and P. S. Ray (1991), A model evaluation of noninductive graupel-ice charging in early electrification of a mountain thunderstorm, *J. Geophys. Res.*, *96*, 12,833–12,855.

C. Barthe and J.-P. Pinty, Laboratoire d'Aérologie, Observatoire Midi-Pyrénées, 14 avenue Edouard Belin, F-31400 Toulouse, France. (barc@aero.obs-mip.fr; pinjp@aero.obs-mip.fr)